

# Mesoscopic atomic entanglement for precision measurements beyond the standard quantum limit

J. Appel , P. J. Windpassinger , D. Oblak , U. B. Hoff , N. Kjærgaard , and E. S. Polzik

Danish National Research Foundation Center for Quantum Optics – QUANTOP, The Niels Bohr Institute, University of Copenhagen, Blegdamsvej 17, DK-2100 København Ø, Denmark.

Submitted to Proceedings of the National Academy of Sciences of the United States of America

**Squeezing of quantum fluctuations by means of entanglement is a well recognized goal in the field of quantum information science and precision measurements. In particular, squeezing the fluctuations via entanglement between two-level atoms can improve the precision of sensing, clocks, metrology, and spectroscopy. Here, we demonstrate 3.4 dB of metrologically relevant squeezing and entanglement for  $\gtrsim 10^5$  cold caesium atoms via a quantum nondemolition (QND) measurement on the atom clock levels. We show that there is an optimal degree of decoherence induced by the quantum measurement which maximizes the generated entanglement. A two-color QND scheme used in this paper is shown to have a number of advantages for entanglement generation as compared to a single color QND measurement.**

spin squeezing | quantum non demolition measurements | entanglement | atomic clocks

When  $N_A$  independent two-level atoms are prepared in an equal coherent superposition of the internal quantum states  $|\uparrow\rangle$  and  $|\downarrow\rangle$ , a measurement of the ensemble population difference  $\Delta N = N_\uparrow - N_\downarrow$  will fluctuate as  $\sqrt{N_A}$  (see Fig. 1A). These fluctuations are referred to as projection noise [1, 2]. More generally, the population difference of the ensemble can be shown to form one component of a collective pseudo-spin vector  $J$ . Taking  $J_z = \frac{1}{2}\Delta N$ , we have the variance  $(\delta J_z)^2 = \frac{1}{4}N_A$  for the case of independent atoms also referred to as a coherent spin state (CSS). The CSS minimizes the Heisenberg uncertainty product so that, e.g.,  $(\delta J_x)^2(\delta J_y)^2 = \frac{1}{4}|\langle J_y \rangle|^2$  where  $\langle J_y \rangle$  is the expectation value of the spin projection operator. At the expense of an increase in  $(\delta J_x)^2$  it is possible to reduce  $(\delta J_z)^2$  (or vice versa) below the projection noise limit while keeping their product constant. This constitutes an example of a spin squeezed state (SSS), for which the atoms need to be correlated. This correlation is ensured to be non-classical if

$$(\delta J_z)^2 < \frac{|\langle J \rangle|^2}{N_A} \Rightarrow \xi \equiv \frac{(\delta J_z)^2}{|\langle J \rangle|^2} N_A < 1, \quad [1]$$

where  $\xi$  defines the squeezing parameter. Under this condition the atoms are entangled [3] and the prepared state improves the signal-to-noise ratio in spectroscopical and metrological applications [1].

Systems of two to three ions have successfully been used to demonstrate spectroscopic performance with reduced quantum noise and entanglement [4, 5]. The situation is somewhat different with macroscopic atomic ensembles where spin squeezing has been an active area of research in the past decade [6, 7, 8, 9, 10, 11, 12, 13]. To our knowledge, no results reporting  $\xi < 1$  via inter-atomic entanglement in such ensembles have been reported so far, with a very recent exception of the paper [14] where entanglement in an external motional degree of freedom of  $2 \cdot 10^3$  atoms via interactions in a Bose-Einstein condensate is demonstrated.

## Spin squeezing by QND measurements

In this article, we report on the generation of an SSS fulfilling Eq. [1] in an ensemble of  $\sim 10^5$  atoms via a QND measurement [7, 15, 16, 17] of  $J_z$ . We show how to take advantage of the entanglement in this mesoscopic system using Ramsey spectroscopy [1] - one of the methods of choice for precision measurements of time and frequency [18] (Fig. 1A). The Figure presents evolution of the pseudo-spin vector  $J$  whose tip is traveling over the Bloch sphere. The Ramsey method allows using the atomic ensemble as a sensor for external fields where the perturbation of the energy difference between the levels  $\Delta E_{\uparrow\downarrow}$  is measured, or as a clock where the frequency of an oscillator is locked to the transition frequency between the two states  $\Omega = \Delta E_{\uparrow\downarrow}/\hbar$ . Fig. 1B illustrates how a suitable SSS can improve the precision of the Ramsey measurement provided that the condition of Eq. [1] is fulfilled.

Here we experimentally demonstrate two crucial steps of the entanglement-assisted Ramsey spectroscopy. First we perform the projection noise squeezing (Fig. 1C) by a QND measurement. Second, using the Ramsey method, we measure the loss of atomic coherence  $|\langle J \rangle|$  due to QND probing. Together these results allow us to demonstrate the condition of Eq. [1]. The complete Ramsey sequence can be achieved if these two steps are supplemented with the rotation of the squeezed ellipse from the equatorial to the meridian plane (see Fig. S1). We pay particular attention to a reliable determination of the projection noise level which is an experimental challenge in its own right. A QND measurement based on far-off resonant dispersive probing is always accompanied by inherent decoherence due to spontaneous emission (shortening of  $|\langle J \rangle|$ , as in Fig. 1B,C) which affects entanglement according to Eq. [1]. As we show in the paper, the ensemble optical depth sets the optimal value of the decoherence which has to be chosen in order to maximize the generated entanglement. We employ a dichromatic QND measurement [19] and show that it has several advantages for the SSS generation [20].

**Experimental Setup.** Cold Cs atoms are loaded into a far off-resonant optical dipole trap (FORT), aligned to overlap with the probe arm of a Mach-Zehnder-Interferometer (MZI, shown in Fig. 2A). The FORT is formed by a Gaussian laser beam with a wavelength of 1032 nm and a power of 2.5 W focussed to a waist of 50  $\mu\text{m}$  inside an evacuated glass cell

## Reserved for Publication Footnotes

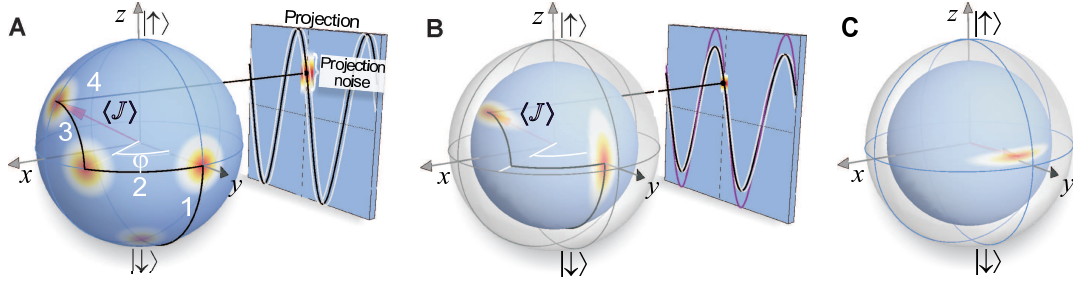


**Fig. 1.** Ramsey spectroscopy with coherent and squeezed states. **A** - Bloch sphere representation of a Ramsey sequence with  $N_A$  atoms initially in the state  $|\downarrow\rangle$  described by a Bloch vector  $\langle J \rangle$  of length  $N_A/2$  pointing towards the south pole. Stage 1: a drive field of frequency  $\nu$  near resonant to the  $|\downarrow\rangle \leftrightarrow |\uparrow\rangle$  transition frequency  $\nu_0$  rotates the Bloch vector to the equator ( $\pi/2$ -pulse) bringing each atom in a superposition state  $\frac{1}{\sqrt{2}}(|\uparrow\rangle + |\downarrow\rangle)$ . This CSS is characterized by quantum fluctuations  $(\delta J_z)^2 = (\delta J_x)^2 = \frac{1}{4}N_A$  illustrated as a fuzzy disk. Stage 2: the atoms evolve freely for a time  $T$  and the Bloch vector precesses about the  $z$  axis by an angle  $\varphi = 2\pi(\nu - \nu_0)T$ .  $\varphi$  is recorded after a second  $\pi/2$ -pulse (stage 3) by measuring the population difference (stage 4):  $\cos \varphi = (N_\uparrow - N_\downarrow)/N_A$ . Projection noise will result in an uncertainty of the Ramsey fringe position. **B** - The effect of projection noise in Ramsey spectroscopy can be reduced by applying an SSS. If the SSS is generated via a dispersive QND measurement the accompanying spontaneous photon scattering leads to a fraction  $\eta$  of decohered atoms thereby reducing the radius of the Bloch sphere and the Ramsey fringe amplitude by a factor  $(1 - \eta)$ . Compared to the CSS shown in **A**, the SSS on the reduced Bloch sphere **B** increases the precision in the determination of  $\varphi$  if the criteria Eq. [1] is fulfilled after the final  $\pi/2$ -pulse. **C** The present paper reports on the squeezing of  $(\delta J_z)^2$ , i.e. along the meridian direction, which can be converted into the squeezing in the equatorial direction by a microwave pulse. The SSS resides on a Bloch sphere of reduced radius as compared to the original CSS.

located in one of the arms of the MZI ([21, 22]). Atoms are loaded into the FORT from a standard magneto-optical trap (MOT) superimposed onto the FORT, which collects and cools atoms from the background vapor to  $\approx 50 \mu\text{K}$ . After loading the FORT, the MOT light is extinguished and a B-field of  $\sim 2$  Gauss is applied, defining a quantization axis orthogonal to the trapping beam. At this stage the atoms occupy the ( $F = 4$ ) ground level but are distributed amongst the magnetic sublevels. To polarize the atoms in one of the clock states, a combination of  $\pi$ -polarized laser light resonant to the  $6S_{1/2}(F = 4) \rightarrow 6P_{3/2}(F' = 4)$  and  $6S_{1/2}(F = 3) \rightarrow 6P_{3/2}(F' = 4)$  transitions is applied, optically pumping the atoms towards the ( $F = 4, m_F = 0$ ) state with 80% efficiency. Purification of clock state atoms proceeds by transferring the ( $F = 4, m_F = 0$ ) state atoms to the ( $F = 3, m_F = 0$ ) state using a resonant  $\pi$ -pulse on the clock transition and blowing away remaining atoms residing in the ( $F = 4$ ) level with light on the  $6S_{1/2}(F = 4) \rightarrow 6P_{3/2}(F' = 5)$  cycling transition. The Coherent Spin State preparation is completed by putting the ensemble in an equal superposition of the clock states  $\bigotimes_{i=1}^{N_A} \left[ \frac{1}{\sqrt{2}}(|\downarrow\rangle + |\uparrow\rangle) \right]_i$  by applying a resonant  $\pi/2$  microwave pulse at the clock frequency. Next we perform successive QND measurements on the sample, after which all atoms are pumped into the  $F = 4$  level to determine the total atom number  $N_A$ . The sequence is repeated several thousand times for various  $N_A$ . A schematic representation of the experimental sequence is shown in Fig. 3A.

**Measurement of the projection noise.** The dispersive measurement of the clock state population difference [23, 24] is realized by detecting the state dependent phase shift of off-resonant probe laser light. In the present experiment one probe  $P_\downarrow$  is coupled to the state  $|\downarrow\rangle \equiv 6S_{1/2}(F = 3, m_F = 0)$ , while a second probe  $P_\uparrow$  is coupled to the state  $|\uparrow\rangle \equiv 6S_{1/2}(F = 4, m_F = 0)$  (see Fig. 2B).

The two probe beams enter the interferometer through different ports, so that the phase shifts imprinted on them by the atoms contribute with opposite signs to the differential signal  $\Delta n$  from the detectors  $D_1, D_2$ . As discussed below this geometry together with a suitable choice of probe detunings provides compensation of a deleterious probe-induced shift of the measured frequency  $\Omega$ . Denoting the sum phototsignal as

$n$  we define

$$\phi = \frac{\Delta n}{n} = \frac{\delta n}{n} + k_\uparrow N_\uparrow - k_\downarrow N_\downarrow, \quad [2]$$

where  $\delta n = \delta n_\uparrow + \delta n_\downarrow$  denotes the total shot noise contribution of both probe colors. The probes are of equal intensity and their detunings are chosen such that the coupling constants  $k \equiv k_\uparrow = k_\downarrow$  are equal. Hence the normalized differential signal  $\phi$  yields a  $J_z$  measurement with the optical shot noise added:

$$\begin{aligned} \phi &= \frac{\delta n}{n} + k\Delta N = \frac{\delta n}{n} + 2kJ_z, \\ \text{var}(\phi) &= \frac{1}{n} + k^2 \text{var}(\Delta N). \end{aligned} \quad [3]$$

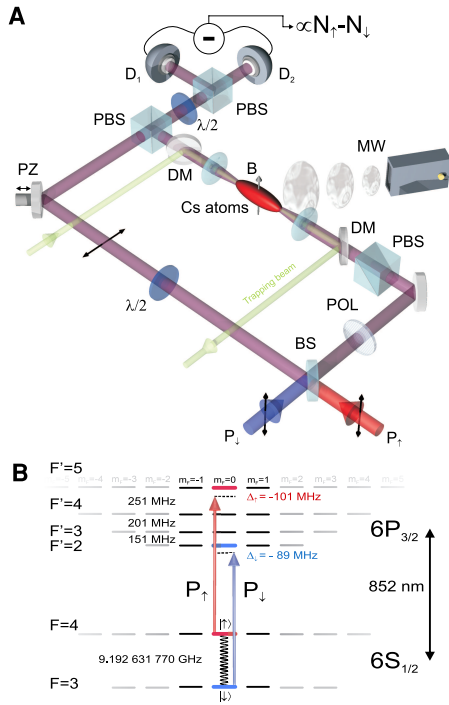
For atoms in a CSS we have  $\text{var}(\Delta N) = N_A$  and Eq. [4] predicts a *linear* increase of the projection noise with the number of atoms.

Figure 4 shows that we have observed the projection noise of atoms as evidenced by the almost perfect linear fit to the noise data (blue points). To further confirm that the linear part of Fig. 4 is the quantum projection noise we verify the value of  $k^2$  for the inferred projection noise slope by independent means (see Supplementary information). Achieving this linearity is a demanding experimental task because it requires technical noise, e.g., fluctuations of the probe power and the interferometer length to affect  $\Delta N$  measurements well below the level of  $1/\sqrt{N_A} \approx 2 \cdot 10^{-3}$  over the time scale of the experiment.

**Conditional noise reduction by QND measurement.** The ability to measure the atomic spin projection with a sensitivity limited by the shot noise of light allows us to produce a conditionally spin squeezed atomic state. After preparation of a CSS, we use  $n_1$  photons to measure  $J_z$  as outlined above and obtain a measurement result  $\phi_1$ , which is randomly distributed around zero with a variance  $\frac{1}{n_1} + k^2 N_A$  (see Eq. [4], blue dots in Fig. 4).

Using the information obtained in the first measurement we can, to a certain degree, predict the outcome  $\phi_2$  of a successive  $J_z$  measurement performed on the same ensemble of atoms. The best estimate for  $\phi_2$  is  $\zeta\phi_1$ , which results in a conditionally reduced variance

$$\text{var}(\phi_2 - \zeta\phi_1) = \frac{1}{n_2} + \frac{1}{1 + \kappa^2} k^2 N_A, \quad [5]$$



**Fig. 2. Experimental setup.** **A**  $\sim 10^5$  Cs atoms cooled to  $\sim 50 \mu\text{K}$  are confined in one arm of a MZI by a trapping beam with the waist of  $50 \mu\text{m}$  folded by two dichroic mirrors (DM). The atoms are prepared in a coherent superposition of the clock states  $|\uparrow\rangle$  and  $|\downarrow\rangle$ , by applying a microwave (MW)  $\pi/2$ -pulse. Two linearly polarized probe beams  $P_\uparrow$  and  $P_\downarrow$  enter the interferometer via separate ports of the input beam splitter (BS). The probes focused to the waist of  $27 \mu\text{m}$  acquire phase shifts proportional to the number of atoms in the clock states  $N_\uparrow$  and  $N_\downarrow$ , respectively. An arrangement of polarizers (POL), polarizing beam splitters (PBS), and half wave plates ( $\lambda/2$ ) is used to adjust the powers and polarizations of the probe and reference beams. The combined phase shift ( $\propto N_\uparrow - N_\downarrow$ ) of the two probes is measured in a balanced homodyne configuration. **B** - Simplified level scheme of Cs showing the D2 line and the detunings of the clock state sensitive probes,  $P_\uparrow$  and  $P_\downarrow$ .

that displays a reduction of the projection noise by  $\frac{1}{1+\kappa^2}$  (cf. red diamonds in Fig. 4). The measurement strength  $\kappa^2 = n_1 k^2 N_A$  describes the ratio of the atomic noise to the shot noise of light and  $\zeta = \text{cov}(\phi_1, \phi_2) / \text{var}(\phi_1) = \kappa^2 / (1 + \kappa^2)$ . A QND measurement with a finite strength  $\kappa^2$  leads to a finite correlation between the two measurements, as shown in Fig. 3B. For  $\kappa^2 = 3.2$  observed for  $N_A = 1.2 \cdot 10^5$  atoms we expect a conditionally reduced variance of  $-6.2 \text{ dB}$  with respect to the projection noise level. In the experiment we find the value  $-(5.3 \pm 0.7) \text{ dB}$  as shown in Fig. 4.

**Decoherence.** Spontaneous emission caused by the QND probes is a fundamental irreversible decoherence mechanism which affects the SSS in two ways. First, it can change the value of  $J_z$  by redistributing atomic populations via inelastic Raman scattering. This effect would be particularly important if a single QND probe coupled to both clock levels were used. Except for special cases such as discussed in [25], the single color probing causes Raman scattering between the clock levels. With the two-color QND scheme which we use here the population redistribution between the hyperfine levels is practically absent because of the selection rules and the choice of detunings (atoms in the ground state level  $F = 4$  are predominantly excited to the level  $F' = 5$  and hence cannot decay to the ground state  $F = 3$ , and similarly for the reverse scattering). The effect of the redistribution between the magnetic sublevels within a given hyperfine level on the

projection noise squeezing is very small (estimated to be less than 1%), as also proven by a good agreement between the observed and predicted degree of this squeezing (see the section on dichromatic probing and supplementary information for further discussion of this issue).

The second and main effect of the spontaneous decoherence on entanglement is due to the reduction of the coherence between the clock levels. Both inelastic Raman and elastic Rayleigh spontaneously scattered photons lead to shortening of the mean collective spin vector  $|\langle J \rangle| \rightarrow (1 - \eta)|\langle J \rangle|$  and hence to the reduction in Ramsey fringe amplitude (see Fig. 1B). The degree of spin squeezing as defined by Eq. [1] depends on the fraction  $\eta$  of atoms which decohere as a result of spontaneous photon scattering during dispersive QND probing. The QND measurement strength can be cast as  $\kappa^2 \propto d\eta$  where  $d$  is the resonant optical depth of the sample [26]. This highlights the trade-off between information gained through strong coupling and coherence lost due to spontaneous emission.

An inhomogeneous AC Stark shift due to the transverse intensity profile of the probe beam can, in principle, cause an additional dephasing and decoherence. However, as discussed in the section on dichromatic QND, this deleterious effect is strongly suppressed in our QND sequence.

We determine  $\eta$  via the reduction in the Ramsey fringe amplitude in a separate echo spectroscopy experiment [21, 22]. The technique and results are summarized in Fig. 5. The reduction in echo fringe amplitude as a result of the probe light thus provides an upper bound for the decoherence inflicted.

**Squeezing and entanglement.** The noise measurement data presented in Fig. 4 corresponds to  $\eta = 20\%$  as measured in echo spectroscopy. According to Eq. 1 metrologically relevant spin squeezing and entanglement  $\xi < 1$  for a given  $N_A$  can be claimed if the conditionally reduced variance of the verification measurement (red diamonds in Fig. 4) is less than the projection noise scaled down by the factor  $(1 - \eta)^2$  (dash-dotted line in Fig. 4). In the inset of Fig. 4 we consider the maximum  $N_A$ -bin of the data and plot  $\xi$  versus  $\eta$ , varying the probe photon number by combining consecutive probe pulses (see Methods for details of the data analysis). Maximum squeezing  $\xi = -(3.4 \pm 0.7) \text{ dB}$  is observed with  $\eta = 20\%$ , corresponding to probing the atoms with  $1.3 \cdot 10^7$  photons. The squeezing reduces as  $\eta$  increases further, confirming the notion that though a stronger measurement enables more precise estimation of  $J_z$ , this reduction in spin noise eventually ceases to be spectroscopically relevant as a result of decoherence.

**Dichromatic QND.** A single probe introduces a phase shift of the Ramsey fringe of approximately 0.8 radians due to the Stark shift. If two properly balanced probes  $P_\downarrow$  and  $P_\uparrow$  have the same spatial mode the differential AC-Stark shift of the clock states  $|\downarrow\rangle$  and  $|\uparrow\rangle$  is strongly suppressed and the phase shift of the Ramsey fringe is reduced below the measurement precision. However, even in the presence of inevitable probe fluctuations which lead to a differential Stark shift, this shift does not affect the QND Ramsey sequence. The differential Stark shift caused by the misbalance of the two probes would affect the initial value of  $J_x$ , that is it would add noise to the anti-squeezed component of the spin without affecting the squeezed component.  $J_x$  is not measured in the Ramsey sequence (see eq. S8 in the Supplementary information), and therefore the dichromatic QND method does not lead to a differential light shift of the clock transition [20]. This feature is most important for both the precision and the accuracy in metrological applications.

Another advantage of the two-color probing is due to the fact that, as opposed to the single probe QND schemes [23] where detuning is fixed roughly in the middle between the atomic levels of interest, the detuning of two probes can be adjusted. The detuning is then chosen so that the optimal value of the parameter  $\eta$  is obtained for a photon number around  $10^7$ , a convenient value which minimizes the combined effect of the laser intensity and frequency classical fluctuations. At the same time for a single probe QND the photon number corresponding to the optimal  $\eta$  would be approximately  $10^{10}$ , thus demanding a challenging level of stabilization of the probe power to much better than  $10^{-5}$ .

Finally, we discuss the fundamental advantage of a dichromatic QND measurement with cyclic transitions [20]. Such probing does not add any noise to  $\delta J_z^2$ . Hence, from Eq. [1] together with the theoretical estimate for  $\delta J_z^2$  after the QND measurement, an optimal squeezing of  $\xi_{\min} = \frac{9}{4} \frac{1}{1+\kappa^2} \propto \frac{1}{d}$  is predicted for  $\eta = \frac{1}{3}$ , assuming a large resonant optical depth  $d$ . Note that the optimal experimental value of  $\eta$  as shown in the inset of Fig. 4 is close to, albeit somewhat smaller than, the theoretical optimum.

We emphasize that the theoretical scaling of  $\xi_{\min} \propto d^{-1}$  for the dichromatic QND method using cyclic transitions is more favorable than the scaling  $\xi_{\min} \propto d^{-1/2}$  for a conventional single-color QND scheme with cross-pumping [26].

The probe transitions used in the present paper are not exactly cyclic. The spontaneous emission does not reshuffle atoms between the hyperfine levels but it does cause Raman scattering  $m_F = 0 \rightarrow m_F = \pm 1$  within each hyperfine level. Atoms spontaneously scattered to both  $m_F = 0$  and  $m_F \neq 0$  do not add noise to the QND-assisted Ramsey sequence (see Supplementary information for details). The only additional partition noise of  $J_z$  (less than 1%) which appears after the spontaneous emission is due to slightly different probe coupling to atoms  $m_F = 0$  and  $m_F \neq 0$ . Interestingly, it becomes obvious from this discussion that the atoms which decohered to  $m_F \neq 0$  states are part of the entangled state since if they were removed after the QND measurement the parameter  $\xi$  would grow due to the increased uncertainty of  $\delta J_z^2$ .

**Conclusion and Outlook.** In summary we have demonstrated a reduction of projection noise to  $-(5.3 \pm 0.6)$  dB and metrologically relevant spin squeezing and entanglement of  $-(3.4 \pm 0.7)$  dB on the Cs microwave clock transition. We analyze in detail the role of spontaneous photon scattering in the Ramsey sequence combined with QND measurements and demonstrate the optimal balance between decoherence and the measurement strength for generation of spin squeezing. The measurement precision improves with the number of atoms, hence it is important that we have demonstrated entanglement with the largest to-date number (over  $10^5$ ) of cold and trapped atoms. We show that the dichromatic QND measurement has several advantageous features in the clock and Ramsey spectroscopy settings.

The phase noise of our microwave reference (*HP8341B*) prevented us from a demonstration of the effect of the spin squeezing in a full clock cycle, even for integration times  $< 10^{-4}$  s. We expect to be able to improve on that with a better microwave source.

A crucial parameter defining the degree of spin squeezing generated with the QND method is the resonant optical depth of the atomic ensemble. Here we have shown that significant entanglement can be obtained with a modest optical depth of  $\sim 16$ . The requirement of high optical depth poses a limitation on the applicability of our results to, e.g., projection

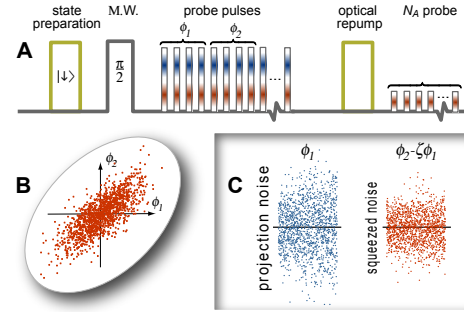


**Fig. 3. Pulse sequence and noise data.** **A** - Atoms are prepared in state  $|\downarrow\rangle$  by an optical pumping sequence and then rotated to the superposition state  $\frac{1}{\sqrt{2}}(|\uparrow\rangle + |\downarrow\rangle)$  by a microwave  $\pi/2$  pulse before the train of 10 probe pulses is applied. Combining the results of several pulses we can change the effective QND measurement strength as explained in the text. The first effective probe pulse measurement result  $\phi_1$  yields the statistics of the  $J_z$  for the CSS. The second effective pulse measurement result  $\phi_2$  verifies the squeezing provided it is sufficiently correlated with  $\phi_1$ .  $N_A$  is measured at the end of each sequence. **B** - Correlations between the first and the second pulse measurements. **C** - the projection noise manifested in the random scattering of about 2000 measurements of  $\phi_1$ ; and the spin squeezed state displayed as the reduced noise in  $\phi_2$  when the QND result is used as  $(\phi_2 - \zeta\phi_1)$

noise limited fountain clocks [18] where the optical depth is usually kept around unity in order to avoid collisional shifts.

Spin squeezing is on the current agenda for optical clocks [27, 28, 29] which are affected by collisions to a much smaller extent. The first step along the lines discussed in the present paper in state-of-the-art lattice clocks has been demonstrated very recently in [30] where a nondestructive measurement using a Mach-Zehnder interferometer with sensitivity near the projection noise level has been reported. The dichromatic QND method can be particularly convenient in optical clocks if both clock levels are probed, because the levels separated by optical energy can be probed with two independent lasers.

In systems with a low single pass optical depth the effective optical depth can be increased by utilizing an optical cavity as demonstrated recently [31] where results similar to ours have been obtained. Sensing and metrology for which a high optical depth and associated collisions are not a problem will probably be the main field of application for this method, unless the collisional shift itself is the goal of a Ramsey experiment [32].

## Methods

**Noise Measurement Sequence.** The clock state sensitive probes  $P_\uparrow$  and  $P_\downarrow$  enter the interferometer via opposite input ports (see Fig. 2) and are phase locked to achieve common mode rejection of frequency fluctuations when probing the atoms. Because of the opposite inputs, the differential output signal  $D_2 - D_1$  for the empty interferometer has opposite signs for  $P_\uparrow$  and  $P_\downarrow$ , and their intensity ratio is controlled as to achieve zero mean of the signal; hence the dichromatic interferometer becomes nearly insensitive to geometric length variations. With the intensity ratio fixed the detunings of  $P_\uparrow$  and  $P_\downarrow$  are fine-tuned to achieve zero mean signal for atoms in the coherent superposition. The two probes are mode matched, so that the transverse spatial distributions of  $P_\uparrow$  and  $P_\downarrow$  (waist size  $27 \mu\text{m}$ ) are very similar. Hence the differential AC Stark shift on the clock transition from a dichromatic probe pulse is significantly reduced across the entire atomic volume.

The geometric path length difference between the probe and reference arms of the interferometer is controlled by a piezo actuated mirror. Prior to atomic probing the mirror position is adjusted in a feedback loop to achieve zero differential interferometer output near the white light position using a sequence of weak auxiliary laser pulses at 840 nm. This light virtually does not interact with the atoms and provides a reference position from which the mirror is subsequently offset to obtain an *individually* balanced output for each of the two probe beams. This allows to reject intensity noise in the probe pulses during superposition state measurements. The off-

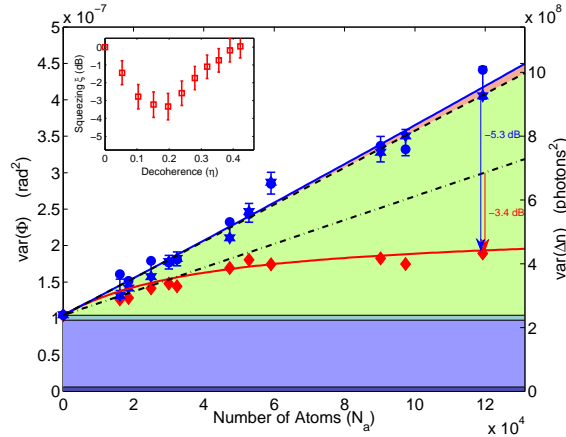


**Fig. 4. Projection noise and spin squeezing.** Blue points, stars: Variances  $\text{var}(\phi_1)$ ,  $\text{var}(\phi_2)$  of the  $J_z$  spin noise measurement of atoms in a CSS versus  $N_A$ , error bars: corresponding statistical uncertainty, centered on  $\frac{1}{2}(\text{var}(\phi_1) + \text{var}(\phi_2))$ ; solid blue line: quadratic fit (see Methods section). Dashed line: CSS projection noise. Dash-dotted line: equivalent CSS projection noise reduced by the loss of atomic coherence. Red diamonds: Conditionally reduced variance of a second  $J_z$  spin measurement predicted by the first:  $\text{var}(\phi_2 - \zeta\phi_1)$ . Red line: reduced noise of SSS predicted from quadratic fits to projection noise data (see Methods section). According to the scaling behavior we classify different noise contributions (see data analysis): Classical fluctuations are represented by the cyan (empty interferometer) and red area (atom-light interaction related). Blue areas: optical shot noise (light blue) and detector noise (dark blue). Green area: projection noise. **Inset:** Spin squeezing  $\xi$  (red boxes) as a function of the decoherence parameter  $\eta$ , corresponding to the fits (dash-dotted black and red line) evaluated for the atom number of the rightmost bin; error bars: standard deviation over analysis runs binning into 5 to 30 groups with respect to  $N_A$ .

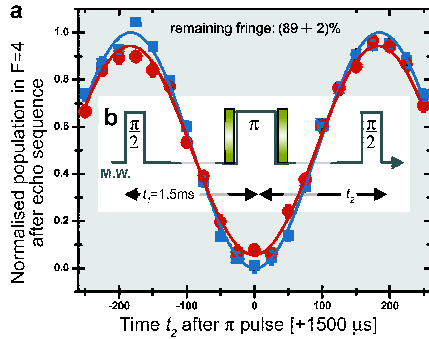


**Fig. 5. Decoherence measurement.** (A) Sample traces of the  $F = 4$  population as function of the second  $\pi/2$ -pulse delay  $t_2$ . Blue squares serve as reference level for the fringe amplitude without any probe light pulses. Red points were obtained with a combined photon number in the two pulses of  $2n_p = 7.4 \cdot 10^6$ . From the fitted curves the reduction of the fringe amplitude is inferred giving an upper bound of  $\eta = (0.11 \pm 0.02)$ . (B) Experimental sequence similar to that of Fig 1a) with addition of a microwave  $\pi$ -pulse to reverse dephasing. Without the probe light pulses, the microwave ( $\pi/2, \pi, \pi/2$ )-pulse sequence compensates all reversible dephasing effects. Absorption of light from the two probe pulses causes a fraction  $\eta$  of atoms to undergo (irreversible) spontaneous emission.

set value depends on the (expected) number of trapped atoms. The atomic ensemble is probed at  $20 \mu\text{s}$  intervals using a sequence of 20 dichromatic pulses with a duration of  $10 \mu\text{s}$  and  $n_{\text{pulse}}$  photons per color, per pulse ( $1.83 \cdot 10^6$  in the probe arm). The differential interferometer signal is sampled on a digital storage oscilloscope from which we determine the differential photon numbers  $\{p_1, p_2, \dots, p_{20}\}$ . After probing the superposition state the interferometer is reset to its reference position and the atoms are optically pumped into the ( $F = 4$ )-level to determine  $N_A$ . The trapped atoms are recycled for additional measurements by re-initializing the ensemble using

optical pumping and purification as described above. During each MOT cycle four ensembles are interrogated and additionally three reference measurements without atoms are recorded.

**Data Analysis.** We combine up to  $P = 10$  successive pulses which allows us to vary the effective QND probe photon number  $n = 2Pn_{\text{pulse}}$ , and obtain the phase shifts  $\phi_1 = (p_1 + \dots + p_P)/n$ ,  $\phi_2 = (p_{P+1} + \dots + p_{2P})/n$ . These measurements are sorted and grouped according to the atom number  $N_A$ . We fit a general quadratic function  $V(N_A) = v_0 + v_1 N_A + v_2 N_A^2$  (solid blue line in Fig. 4) to  $\text{var}(\phi_1)$  and  $\text{var}(\phi_2)$  (blue points and stars) and another function  $C(N_A) = c_0 + c_1 N_A + c_2 N_A^2$  to  $\text{cov}(\phi_1, \phi_2)$  to identify the light noise contribution  $v_0 - |c_0| - d_0$  (light blue area),  $d_0 = \text{detector noise}$  (dark blue area), and the projection noise  $v_1 N_A$  (green field, dashed line). Knowing the outcome of a  $\phi_1$  measurement the best prediction for the successive  $\phi_2$  measurement on the same sample is  $\zeta\phi_1$ , with  $\zeta = \text{cov}(\phi_1, \phi_2)/\text{var}(\phi_1)$ . The conditionally reduced variance  $\text{var}(\phi_2 - \zeta\phi_1)$  (red diamonds) is predicted by  $R(N) = V(N) \left(1 - \left(\frac{C(N)}{V(N)}\right)^2\right)$  (red line). From a spin-echo measurement with pulses of  $n_{\text{se}} = 7.4 \cdot 10^6$  photons altogether resulting in a fringe contrast reduction of  $\eta_{\text{se}} = 11\%$  the value of spin squeezing for a QND measurement employing a total of  $n_{\text{probe}}$  photons in the probe arm is then calculated as  $\text{SQ} = 10 \log_{10} \left( \frac{R(N_{A,\text{max}}) - R(0)}{v_1 N_{A,\text{max}}} (1 - \eta_{\text{se}})^{-2n_{\text{probe}}/n_{\text{se}}} \right)$ . To compensate for slow drifts in our setup, from each set of raw data  $p_1 \dots p_{20}$  we subtract the individual pulse data recorded in the previous MOT cycle and perform our data analysis on the differential values.

#### Decoherence measurement.

In Fig. 5 we show the decoherence measurements for two dichromatic probe light pulses containing in total  $7.4 \cdot 10^6$  photons. The data has been taken at a microwave detuning of  $\Delta\Omega = 3 \text{ kHz}$  from the clock transition frequency and the inversion of the phase through the microwave  $\pi$ -pulse was induced after 1.5 ms of free evolution. The two light pulses reduce the echo-fringe by  $11 \pm 2\%$  and thus this forms an upper bound for  $\eta$  for the combined effect of these probe pulses. From this we can deduce the decoherence  $\eta$  corresponding to a probe pulse with a photon number  $n_P$  as  $\eta(n_P) \approx 1 - (1 - 0.11)^{\frac{n_P}{7.4 \cdot 10^6}}$ .

We have also verified that the dichromatic probing employed in the QND measurement indeed provides a significant reduction of the differential Stark shift by measuring the fringe visibility reduction in the absence of the  $\pi$ -pulse. In cases when the two probes were mode matched to better than 97% we indeed observed an identical fringe reduction irrespectively of the  $\pi$ -pulse.

#### Appendix: Derivation of the QND measurement equation

To describe the propagation of the probe light through the atomic gas, we express its complex valued susceptibility by

$$\chi = \frac{n_A \lambda}{L} \frac{1}{2\pi} Q, \quad Q = -\frac{3\lambda^2}{4\pi} \sum_l \frac{\wp_l}{\Delta_l/\gamma + i/2}, \quad [6]$$

where for each probe color the sum is taken over all possible transitions;  $\wp_l$  denote Clebsch-Gordan coefficients,  $\Delta_l$  is the detuning from resonance,  $n_A$  is the atom column density,  $L$  is the interaction length,  $\lambda$  is the vacuum wavelength, and  $1/\gamma$  the excited state lifetime.

Since the  $P_\uparrow$  ( $P_\downarrow$ ) probe only interacts with atoms in the  $|\uparrow\rangle$  ( $|\downarrow\rangle$ ) state we can calculate the phase shift  $\theta$  and absorption  $e^{-\alpha}$  for a plane wave of the probe light passing through the cloud as follows:

$$\theta_{\uparrow,\downarrow} = \frac{1}{2} \text{Re} \frac{2\pi}{\lambda} L \chi_{\uparrow,\downarrow} = \frac{1}{2} n_{A\uparrow,\downarrow} \text{Re} Q_{\uparrow,\downarrow}, \quad [7]$$

$$\alpha_{\uparrow,\downarrow} = \text{Im} \frac{2\pi}{\lambda} L \chi_{\uparrow,\downarrow} = n_{A\uparrow,\downarrow} \text{Im} Q_{\uparrow,\downarrow}. \quad [8]$$

The Gaussian spatial profiles of the two probes  $I_P(r) = \frac{2}{\pi w^2} e^{-2\frac{r^2}{w^2}}$  with a waist size  $w = 27 \mu\text{m}$  are mode matched to better than 97% by maximizing the interference fringe between the two spatial modes using the same laser as input. The atomic cloud is laser cooled and trapped in a far detuned dipole trap, as described in detail in [21], so that the transverse size of the cloud is about a factor of two larger than

the probe cross section, hence the total column density  $n_A$  is considered constant across the probe cross section.

$n_A$  can be expressed as the *sum* of the column densities of the individual states:

$$n_A = n_{A\uparrow}(r, \vartheta) + n_{A\downarrow}(r, \vartheta) \quad [9]$$

Due to quantum fluctuations in the *difference* of the populations in the  $|\uparrow\rangle$  and  $|\downarrow\rangle$  states, the individual contributions  $n_{A\uparrow,\downarrow}(r, \vartheta)$  can differ for different positions  $(r, \vartheta)$  within the beam.

The measurement of the probe phase shift is performed by interference with a mode matched reference beam and hence the differential number of photons measured by the detectors  $D_1, D_2$  is given by

$$\Delta n_{\uparrow,\downarrow} = \pm 2\sqrt{tn_{R\uparrow,\downarrow}n_{P\uparrow,\downarrow}}\theta_{\uparrow,\downarrow}, \quad [10]$$

$$\text{where } \theta_{\uparrow,\downarrow} = \frac{1}{2}\text{Re}Q_{\uparrow,\downarrow} \int \int_0^{2\pi} d\vartheta dr I(r)n_{A\uparrow,\downarrow}(r, \vartheta) \quad [11]$$

is the spatially averaged phase shift of the probe(s),  $t = 63\%$  is the probability of the homodyne detection of a photon which has interacted with the clock atoms,  $n_R$  is the number of detected photons from the reference arm of the interferometer,  $n_P$  is the number of probe photons interacting with atoms, and  $n_{A\uparrow,\downarrow}$  is the column density of the atomic cloud in the two clock states respectively. Since the probes are injected via opposite input ports, the detector signals have opposite signs. In deriving Eq. [11] we assumed that the phase shifts  $\theta_{\uparrow,\downarrow}$  are small such that  $\sin(\theta_{\uparrow,\downarrow}) \approx \theta_{\uparrow,\downarrow}$ .

The photon numbers for both probes are matched ( $n_R \equiv n_{R\uparrow} = n_{R\downarrow}$ ,  $n_P \equiv n_{P\uparrow} = n_{P\downarrow}$ ) whereas the detunings are chosen such that the differential number of photoelectrons (the signal) for the two probes is zero for equal populations of the clock levels, i.e.,  $\text{Re}Q_{\uparrow} = \text{Re}Q_{\downarrow}$ . Hence with  $\tilde{n} \equiv \sqrt{tn_R n_P} Q$  denoting the interferometer fringe amplitude the total signal due to atoms can be expressed as

$$\Delta n = \tilde{n} \left[ \text{Re}Q \int \int_0^{2\pi} d\vartheta dr I_P(r) \left( n_{A\uparrow}(r, \vartheta) - n_{A\downarrow}(r, \vartheta) \right) \right]. \quad [12]$$

When the atoms are prepared in one of the clock states, say state  $|\uparrow\rangle$ , the interferometer signal measures the total number of probed atoms  $\Delta n_{|\uparrow\rangle} = n_{A\uparrow} \tilde{n} \text{Re}Q$ .

When the clock atoms are prepared in a coherent superposition of the states  $|\uparrow\rangle$  and  $|\downarrow\rangle$  (the CSS), the expectation value for the signal is zero:  $\langle \Delta n_{\text{CSS}} \rangle = 0$ . Since the CSS is a product state there is no correlation in the noise of  $n_{A\uparrow} - n_{A\downarrow}$  at different positions within the beam and therefore (omitting optical shot noise for the rest of this section):

$$\begin{aligned} \text{var}(\Delta n_{\text{CSS}}) &= \tilde{n}^2 (\text{Re}Q)^2 \text{var} \left[ \int \int_0^{2\pi} d\vartheta dr I_P(r) (n_{A\uparrow}(r, \vartheta) - n_{A\downarrow}(r, \vartheta)) \right] \\ &= \tilde{n}^2 (\text{Re}Q)^2 \int \int_0^{2\pi} d\vartheta dr I_P(r)^2 \text{var} [n_{A\uparrow}(r, \vartheta) - n_{A\downarrow}(r, \vartheta)] \\ &= \tilde{n}^2 (\text{Re}Q)^2 \frac{n_A}{\pi w^2}. \end{aligned} \quad [13]$$

This motivates the definitions

$$\begin{aligned} N_{\uparrow,\downarrow} &\equiv \int \int_0^{2\pi} d\vartheta dr I_P(r) (\pi w^2 n_{A\uparrow}(r, \vartheta)), \\ N_A &\equiv \pi w^2 n_A, \quad n \equiv 2(n_R + tn_P), \quad k \equiv \frac{\tilde{n} \text{Re}Q}{n\pi w^2} \end{aligned} \quad [14]$$

so that from Eq. [12] we can derive Eq.[3]:  $\phi = \frac{\Delta n}{n} = k\Delta N$ . We find consistently that for all atoms in the state  $|\uparrow\rangle$ :  $\phi_{|\uparrow\rangle} = kN_{\uparrow} = kN_A$  and for the CSS:  $\langle \phi_{\text{CSS}} \rangle = 0$ ,  $\text{var}(\phi_{\text{CSS}}) = k^2 \text{var}(\Delta N) = k^2 N_A$ .

**ACKNOWLEDGMENTS.** The work was funded by the Danish National Research Foundation, by EU grants COMPAS, EMALI, and QAP. N.K. gratefully acknowledges support from the Danish Natural Science Research Council via a Steno Fellowship. We thank R. Le Targat and J.H. Müller for helpful discussions.

## References

- Wineland DJ, Bollinger JJ, Itano WM, Moore FL, Heinzen DJ (1992) Spin squeezing and reduced quantum noise in spectroscopy. *Phys. Rev. A* 46:R6797–R6800.
- Kitagawa M, Ueda M (1993) Squeezed spin states. *Phys. Rev. A* 47:5138–5143.
- Sørensen A, Duan LM, Cirac JI, Zoller P (2001) Many-particle entanglement with Bose-Einstein condensates. *Nature* 409:63–66.
- Leibfried D, *et al.* (2004) Toward Heisenberg-limited spectroscopy with multiparticle entangled states. *Science* 304:1476–1478.
- Roos CF, Chwalla M, Kim K, Riebe M, Blatt R (2006) ‘Designer atoms’ for quantum metrology. *Nature* 443:316–319.
- Hald J, Sørensen JL, Schori C, Polzik ES (1999) Spin squeezed atoms: A macroscopic entangled ensemble created by light. *Phys. Rev. Lett.* 83:1319–1322.
- Kuzmich A, Mandel L, Bigelow NP (2000) Generation of spin squeezing via continuous quantum nondemolition measurement. *Phys. Rev. Lett.* 85:1594–1597.
- Orzel C, Tuchman AK, Fenselau ML, Yasuda M, Kasevich MA (2001) Squeezed states in a bose-einstein condensate. *Science* 291:2386–2389.
- Sørensen A, Molmer K (2001) Entanglement and extreme spin squeezing. *Phys. Rev. Lett.* 86:4431–4434.
- Andre A, Sørensen A, Lukin M (2004) Stability of atomic clocks based on entangled atoms. *Phys. Rev. Lett.* 92:230801.
- Gerbier F, Fölling S, Widera A, Mandel O, Bloch I (2006) Probing number squeezing of ultracold atoms across the superfluid-Mott insulator transition. *Phys. Rev. Lett.* 96:090401.
- Fernholz T, *et al.* (2008) Spin squeezing of atomic ensembles via nuclear-electronic spin entanglement. *Phys. Rev. Lett.* 101:073601.
- Takano T, *et al.* (2009) Spin squeezing of a cold atomic ensemble with the nuclear spin of one-half. *Phys. Rev. Lett.* 102:033601.
- Estève J, Gross C, Weller A, Giovanazzi S, Oberthaler MK (2008) Squeezing and entanglement in a Bose-Einstein condensate. *Nature* 455:1216–1219.
- Guerlin C, *et al.* (2007) Progressive field-state collapse and quantum non-demolition photon counting. *Nature* 448:889–893.
- Caves CM, Thorne KS, Drever RWP, Sandberg VD, Zimmermann M (1980) On the measurement of a weak classical force coupled to a quantum-mechanical oscillator. I. issues of principle. *Rev. Mod. Phys.* 52:341–392.
- Atature M, Dreiser J, Badolato A, Imamoglu A (2007) Observation of Faraday rotation from a single confined spin. *Nature Physics* 3:101–105.
- Santarelli, G *et al.* (1999) Quantum projection noise in an atomic fountain: A high stability cesium frequency standard. *Phys. Rev. Lett.* 82:4619–4622.
- Kuzmich A, Bigelow NP, Mandel L (1998) Atomic quantum non-demolition measurements and squeezing. *Europhys. Lett.* 42:481–486.
- Saffman M, Oblak D, Appel J, Polzik ES (2008) Spin squeezing of atomic ensembles by multi-color quantum non-demolition measurements. *arXiv:0808.0516*.
- Oblak D *et al.* (2008) Echo spectroscopy of atomic dynamics in a gaussian trap via phase imprints. *Eur. Phys. J. D* 50:67–73.
- Windpassinger PJ, *et al.* (2008) Inhomogeneous light shift effects on atomic quantum state evolution in non-destructive measurements. *New J. Phys.* 10:053032.
- Oblak D, *et al.* (2005) Quantum-noise-limited interferometric measurement of atomic noise: Towards spin squeezing on the Cs clock transition. *Phys. Rev. A* 71:043807.
- Windpassinger PJ, *et al.* (2008) Nondestructive probing of rabi oscillations on the cesium clock transition near the standard quantum limit. *Phys. Rev. Lett.* 100:103601.
- Ozeri R, *et al.* (2005) Hyperfine coherence in the presence of spontaneous photon scattering. *Phys. Rev. Lett.* 95:030403.
- Hammerer K, Sørensen A, Polzik ES (2008) Quantum interface between light and atomic ensembles. *arXiv:0807.3358*.
- Meiser D, Ye J, Holland M (2008) Spin squeezing in optical lattice clocks via lattice-based QND measurements. *New J. Phys.* 10:073014.
- Wilpers G, *et al.* (2002) Optical clock with ultracold neutral atoms. *Phys. Rev. Lett.* 89:230801.

29. Ludlow AD *et al.* (2008) Sr lattice clock at  $10^{-16}$  fractional uncertainty by remote optical evaluation with a Ca clock. *Science* 319:1805–1808.
30. Lodewyck J, Westergaard PG, Lemonde P. Non-destructive measurement of the transition probability in a Sr optical lattice clock. *quant-ph:0902.2905*
31. Schleier-Smith MH, Leroux ID, Vuletić V (2008) Reduced-quantum-uncertainty states for an atomic clock. *arXiv:0810.2582v1*.
32. Hart RA, Xu X, Legere R, Gibble K (2007) A quantum scattering interferometer. *Nature* 446:892–895.

## Supplementary Information

# Mesoscopic atomic entanglement for precision measurements beyond the standard quantum limit

**Verification of the Projection Noise level.** We perform projection noise measurements on a CSS to obtain fluctuating phase shifts  $\phi_{\text{CSS}}$  with  $\text{var}(\phi_{\text{CSS}}) = k^2 \text{var}(\Delta N) = k^2 N_A$ . After each measurement we pump all the atoms into the  $|\uparrow\rangle$  state and determine the phase shift  $\phi_{|\uparrow\rangle} = kN_{\uparrow} = kN_A$ . These relations allow us to determine the maximum effective number of atoms from the maximum phase shift observed  $\phi_{|\uparrow\rangle, \text{max}}$ :

$$N_{A, \text{max}} = \phi_{|\uparrow\rangle, \text{max}} \cdot \left( \frac{d\text{var}(\phi_{\text{CSS}})}{d\phi_{|\uparrow\rangle}} \right)^{-1} = 1.2 \cdot 10^5. \quad [\text{S1}]$$

An independent way to determine  $N_A$  is described as follows: We determine  $Q$  from

$$Q_{\uparrow} = -\frac{3\lambda^2}{4\pi} \gamma \left[ \frac{5/9}{\Delta_{\uparrow} + i\gamma/2} + \frac{1/9}{\Delta_{\uparrow} + 452 \text{ MHz} + i\gamma/2} \right] \quad [\text{S2}]$$

and by inserting the probe beam radius  $w$  into definition given in Eq. [14] of the main text together with Eq. [7] the maximum effective atom number can be deduced from the maximum phase shift  $\phi_{|\uparrow\rangle, \text{max}} = 0.18 \text{ rad}$ :

$$N_{A, \text{max}} = \phi_{|\uparrow\rangle, \text{max}} \cdot \frac{2\pi w^2}{\text{Re } Q_{\uparrow}} = 1.8 \cdot 10^5. \quad [\text{S3}]$$

The values obtained from eq. [S1] and eq. [S3] show reasonable agreement, considering that the approximation that the atomic cloud is wide compared to the probe beam but its axial extension is small compared to the probe beam Rayleigh length are only approximately fulfilled. The projection noise slope  $\frac{d\text{var}(\phi_{\text{CSS}})}{d\phi_{|\uparrow\rangle}}$  obtained in different experimental runs over the course of several weeks shows a reproducibility to within  $\pm 10\%$ .

**Consistency check of the atom number estimation.** Let  $\alpha_{\uparrow, \text{CSS}}$  denote the absorption coefficient of a cloud of atoms, prepared in the CSS for the two probe wavelengths. The overall absorption coefficient for a dichromatic light pulse can then be expressed as

$$\alpha_{\text{CSS}} = \frac{\alpha_{\uparrow, \text{CSS}} + \alpha_{\downarrow, \text{CSS}}}{2} = n_A \frac{\text{Im } Q_{\uparrow} + \text{Im } Q_{\downarrow}}{4}. \quad [\text{S4}]$$

A light pulse with  $2n_P$  photons interacting with the atoms causes  $\alpha_{\text{CSS}} \cdot 2n_P$  scattering events. Each photon scattered off an atom that is still in the superposition state reveals this atom's internal state and therefore ruins the superposition. Thus for each scattered photon per unit area the density  $n_{\text{CSS}}(r, \vartheta)$  of atoms that still reside coherently in the  $(|\uparrow\rangle + |\downarrow\rangle)/\sqrt{2}$  superposition is reduced by  $n_{\text{CSS}}/n_A$ . Hence for a pulse with the photon column density  $2n_P I_P(r)$  one can derive the differential equation

$$dn_{\text{CSS}} = -\alpha_{\text{CSS}} \frac{n_{\text{CSS}}}{n_A} I_P 2 dn_P, \quad [\text{S5}]$$

which has the solution

$$n_{\text{CSS}}(n_P) = n_A \exp \left( -\alpha_{\text{CSS}} I_P \frac{2n_P}{n_A} \right). \quad [\text{S6}]$$

The last step of the spin-echo sequence outlined above is the measurement of the decoherence parameter  $\eta = 1 - N_{\text{CSS}}/N_A$  by determining the fraction of atoms that still form a CSS, weighted with the probe beam profile  $I_P(r)$ :

$$\eta = 1 - \frac{N_{\text{CSS}}}{N_A} = 1 - \int_0^{2\pi} \int_0^{\infty} d\vartheta r dr I_P(r) \frac{n_{\text{CSS}}}{n_A} = 1 - \int_0^{2\pi} \int_0^{\infty} d\vartheta r dr I_P(r) \exp \left( -2n_P I_P(r) \frac{\text{Im } Q_{\uparrow} + \text{Im } Q_{\downarrow}}{4} \right). \quad [\text{S7}]$$

Using  $w = 27 \mu\text{m}$ ,  $2n_P = 7.4 \cdot 10^6$  for our probe frequencies eq. [S7] predicts  $\eta = 17\%$ . This estimate becomes closer to the the observed value of 11% when optical losses induced by the vacuum cell windows and the spatial profile of the atomic density within the probe volume are taken into account.

**The clock operation and the effect of spontaneous emission on the dichromatic QND measurement.** In this section we outline a Ramsey-sequence which would allow the squeezed state created by the dichromatic QND measurement to improve on the clock performance. This is essentially the sequence depicted in Fig. S1A-C. Consider a CSS pointing along the  $y$ -axis on the Bloch sphere (Fig. S1A). We perform a QND measurement of  $J_z$  and then apply the sequence S:  $\pi/2$  – rotation about  $y$ -axis,  $\varphi$  precession about  $z$ -axis,  $\pi/2$  – rotation about  $x$ -axis.

This transformation corresponds to the unitary operator  $\hat{U}(\varphi) = \exp\left(-i\frac{\pi}{2}\hat{J}_x\right)\exp\left(-i\varphi\hat{J}_z\right)\exp\left(i\frac{\pi}{2}\hat{J}_y\right)$ . In the Heisenberg picture a final  $J_z$  measurement performed after completion of the S sequence can be related to the initial  $J_z$  operator as follows:

$$\hat{J}_z^{\text{final}}(\varphi) = \hat{U}^\dagger(\varphi)\hat{J}_z^{\text{initial}}\hat{U}(\varphi) = \cos\varphi\hat{J}_z^{\text{initial}} - \sin\varphi\hat{J}_y^{\text{initial}} \quad [\text{S8}]$$

so that the expectation value  $\langle\hat{J}_z^{\text{final}}(\varphi)\rangle = \cos\varphi\langle\hat{J}_y^{\text{initial}}\rangle$  can be used to determine the precession angle  $\varphi$ . The highest sensitivity to changes of  $\varphi$  is achieved when  $\varphi = -\pi/2$ . For this angle, however, the projection noise  $\text{var}\left(\hat{J}_z^{\text{final}}(\varphi)\right) = \sin\varphi\text{var}\left(\hat{J}_z^{\text{initial}}\right)$  is also maximal. By making use of the QND measurement of  $J_z^{\text{initial}}$  prior to the sequence S we can reduce these fluctuations conditionally. For  $\varphi = -\pi/2$  equation [S8] reduces to  $\hat{J}_z^{\text{final}}(-\pi/2) = \hat{J}_z^{\text{initial}}$  which means that the spin projection along the  $z$ -axis is invariant under this sequence and the outcome of a measurement of  $J_z^{\text{final}}$  after the sequence S can be predicted up to the uncertainty following the QND measurement of  $J_z^{\text{initial}}$ .

The invariance of  $J_z$  in the proposed clock sequence has an important implication for the influence of the atoms that have been decohered by spontaneous scattering of photons from the QND probe pulse. The key point is that in our scheme, each of the two probes couples to one ground level population only: The selection rules restrict spontaneously scattered atoms to decay back to the hyperfine level they were initially in. Since the two probes measure the populations in the whole hyperfine manifolds, i.e. one detects  $N_\uparrow$  ( $F = 4$ , all sublevels) while the other detects  $N_\downarrow$  ( $F = 3$ , all sublevels), the measured value of  $J_z = \frac{1}{2}(N_\uparrow - N_\downarrow)$  is, to first order, immune to spontaneous scattering.

Moreover, the clock sequence S only affects atoms in states  $m_F = 0$  because atoms in all other states are not coupled to the microwave field and thus do not perform any of the rotations. This isolation is due to their resonant microwave frequencies being shifted with respect to the  $F = 4, m_F = 0 \leftrightarrow F = 3, m_F = 0$  transition frequency by a bias magnetic field. Therefore the contribution of these atoms to the measured  $J_z$  is also invariant under the clock sequence. The conclusion is that the total  $J_z$  measured by the dichromatic QND method is invariant under the clock sequence S irrespectively of the spontaneous emission, and hence its contribution to the noise of the clock measurement can be effectively reduced by this approach.

A deviation from the above description comes from the fact that the  $\pi$ -polarized probes couple slightly differently to  $m_F = 0$  and  $m_F = \pm 1$  levels. This adds some small extra noise to the spin squeezed state, which in principle could even be avoided by repumping all atoms with  $m_F \neq 0$  into the according  $m_F = 0$  state.

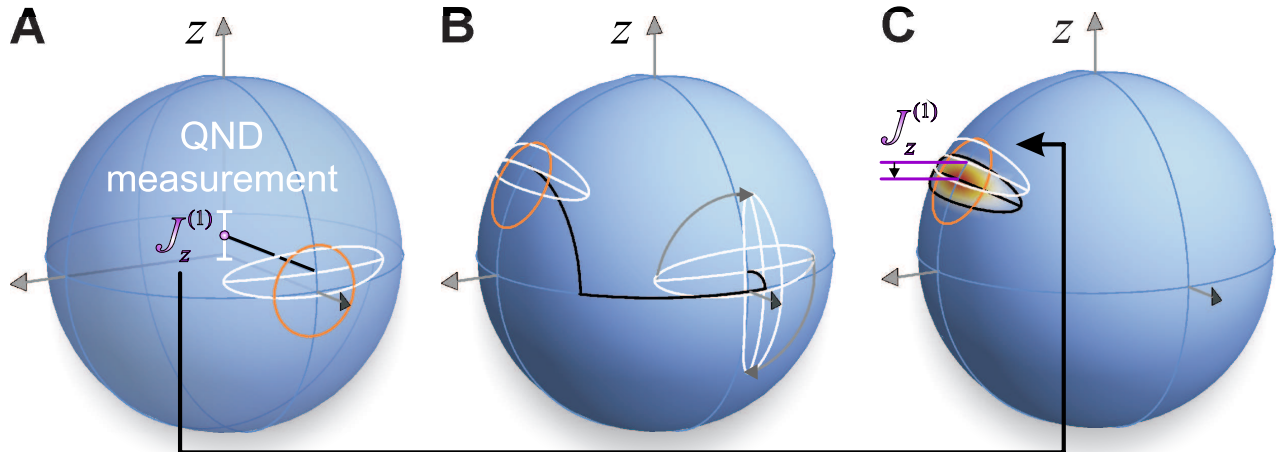


**Fig. S1.** (A) A QND measurement of  $J_z$  with result  $J_z^{(1)}$  creates an SSS displaced from the equator. (B) The SSS is rotated about the  $y$  axis and the Ramsey sequence proceeds as in Fig. 1A in the main paper. (C) The projection noise uncertainty of the clock signal can be reduced by using the knowledge of  $J_z^{(1)}$ .